Measuring Receiver Benchmark for Conducted and Radiated Emissions Testing in Space Applications

Marco A. Azpúrua
EMC Barcelona
EMC Electromagnetic BCN, S.L.
Barcelona, Spain
0000-0001-8078-5116

Marc Pous
HE Space
for European Space Agency
Noordwijk, the Netherlands
0000-0003-2660-5254

Jordi Solé-Lloveras
EMC Barcelona
EMC Electromagnetic BCN, S.L.
Barcelona, Spain
0000-0003-1631-1172

Dongsheng Zhao
RHEA System
for European Space Agency
Noordwijk, the Netherlands
0000-0002-0262-4963

Ferran Silva
Grup de Compatibilitat Electromagnètica
Universitat Politècnica de Catalunya
Barcelona, Spain
0000-0003-3019-3993

***Abstract*—This paper compares the measurement results obtained from three different implementations of measuring receivers regarding spectral level accuracy. The objective is to validate the suitability of direct sampling electromagnetic emissions measurements with respect to those delivered by a high-end EMI receiver in frequency swept and FFT modes. The experimental setups follow the verification methods described in the ECSS-E-ST-20-07C Rev.2 standard to set realistic and reproducible conditions. Between 50 kHz and 100 MHz, common mode and differential mode currents are measured when multi-sine excitation signals with controlled amplitude profiles are used as references. Subsequently, conducted and radiated emissions tests are run to investigate the correlation between measurements with the different receivers. The instruments used are a low-cost USB digitiser Picoscope PS5444D, a high-performance benchtop oscilloscope R&S RTO6 and the R&S ESW44 full-compliant EMI test receiver. The analysis concludes that the emissions measurements performed with the direct sampling approach are excellent for the intended application, exhibiting an accuracy comparable to the dedicated EMI test receiver and a well-adequate dynamic range and noise level.**

***Index Terms*—accuracy, conducted emissions, direct sampling, measuring receiver, radiated emissions**

I. Introduction

The essential tool for testing electromagnetic emissions is the measuring receiver. It is an "instrument such as a tunable voltmeter, an EMI receiver, a spectrum analyser or a Fast Fourier Transform (FFT)-based measuring instrument, with or without preselection, which meets the relevant parts of this standard," [1]. In the European Cooperation for Space Standardization (ECSS) electromagnetic compatibility (EMC) standard [2] the concept of measurement receivers and spectrum analyser is interchangeable and only amplitude ($\pm 2\,\mathrm{dB}$) and frequency ($\pm 2\,\%$) tolerances are given. In general, EMC standards specify the measuring receiver using a "black-box" approach. This allows diverse architectures of compliant measuring receivers, each with advantages and drawbacks.

Firstly, there are conventional swept receivers with super-heterodyne architecture that fundamentally measure the signal within a fixed resolution bandwidth in a given measurement time, which results in a long scan time for obtaining the amplitude of the spectrum in the entire frequency range. They are not suitable for assessing transient and time-varying phenomena since each frequency step corresponds to different instants. As for the benefits, they can reach a superb dynamic range while handling high- and low-level inputs. Likewise, there are the FFT-based measuring receivers that take advantage of time-domain measurements to speed up emissions testing and provide time-frequency analysis features, which help evaluate and mitigate interference from transient, time-varying, and stochastic electromagnetic disturbances [3], [4]. Currently, real-time analysers [5], [6], and direct-sampling (DS) implementations using oscilloscopes [7], [8] are two distinct approaches used for FFT-based measuring receivers. Then, more recently, software-defined radio (SDR) modules have been adapted to perform pre-compliance radiated electromagnetic emissions measurements [9], [10]. SDR modules have excellent price–performance, are highly configurable and have good open-source resources.

With all this diversity in mind, one may wonder how good the aforementioned measuring receiver architectures are when compared to each other. In [11], the author provides an insightful theoretical analysis comparing direct sampling versus heterodyne radio frequency (RF) receivers. This study argues DS RF receivers could be as good as analog heterodyne receivers in terms of the effective number of bits (ENOB), the Schreier figure-of-merit and power efficiency for equal dynamic range specifications. Also, the performance of DS (full time-domain) EMI measurement systems has been investigated through extensive calibrations and verifications following a metrology approach [12], [13]. The reported results support that, provided the correct signal processing and adequate hardware specifications, oscilloscope-based measurements comply

with the relevant CISPR 16-1-1 baseline requirements. Other studies have benchmarked FFT and stepped scan test receivers as part of actual testing scenarios, including CISPR 32 testing of real equipment [14], in-situ emissions assessments of atypical equipment [15], [16], and common- and differential mode conducted emissions measurements [17].

However, in most cases, the answer will be relative to the intended application. In particular, the space sector applies specific EMC requirements and standards, e.g. the ECSS-E-ST-20-07 [2] and the MIL-STD-461G [18]. As for the measurement receiver, EMI testing for space systems uses frequency ranges, resolution bandwidths and dwell times that differ from CISPR standards. More importantly, the EMC plan can vary from mission to mission. For instance, previous works exploited the multichannel capabilities of full time-domain EMI measurement systems in the characterization of magnetic field emissions of a reaction wheel [19] or benefited from the extremely fast response of real-time analysers to increase the probability of interception of short events occurring during nanosatellites emissions testing [20].

This paper goes a step forward in comparing the measurement results obtained from three different implementations of measuring receivers regarding spectral level accuracy. The goal is to validate direct sampling EMI measurements under space application conditions with respect to those delivered by a high-end EMI receiver in frequency swept and FFT modes. Section II describes the methodology, including the experimental setup and the measuring receivers considered. Next, Section III presents the results obtained for test receivers and their comparative analysis.

II. Methodology

The measurement campaign explained in what follows was carried out in the EMC Laboratory of ESA-ESTEC, Noordwijk, the Netherlands. This section describes the experimental setup and the different test subjects benchmarked.

A. Experiment 1: CE verification

Fig. 1 shows a block diagram of the experiment. It is similar to the verification setup for the conducted emissions (CE) tests as defined in [2] for power and signal leads in the 50 kHz - 100 MHz range.

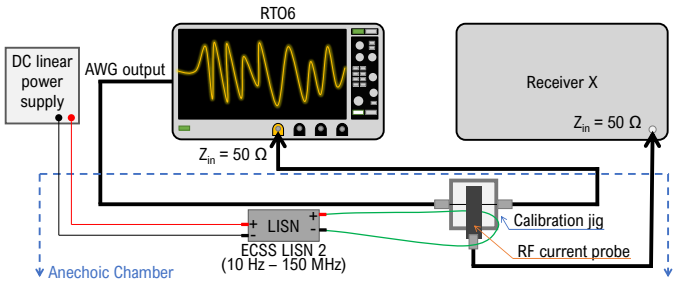

Fig. 1. Block diagram of the test setup: Experiment 1.

In this case, the reference current level is directly measured by placing the oscilloscope in series in the same loop as the current probe and the calibration jig. The excitation is a multisine wave synthesised with an arbitrary waveform generator (AWG) of the RTO6. The DC supply delivers 1 A for checking undesired saturation effects. The Receiver X in the diagram represents one of the test objects defined in the next subsection. Nothing but the receiver is changed in between successive measurements. Two measurement sets were performed, one for each RF current probe used, that is, models 6741-1 (10 kHz - 100 MHz) and 9145-1 (10 kHz - 152 MHz) both from Solar Electronics Company.

B. Experiment 2: CE and RE testing

Conducted and radiated emissions measurements were performed on DC/DC power converter modules. For CE, the test setup employed is depicted in Fig. 2 diagram. Likewise, for the radiated emissions (RE) test, a sketch of the experimental setup is shown in Fig. 3.

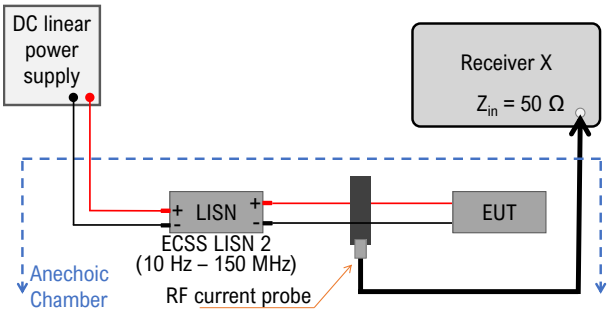

Fig. 2. Block diagram of the test setup: Experiment 2, CE testing.

Two different EUTs were considered, namely, EUT_1 and EUT_2. EUT_1 is a highly efficient DC/DC GaN buck converter (48 V to 12 V) based on the GS61008P GaN Systems' transistors and switching at 1 MHz. EUT_1 circuit neither includes specific EMI filters nor shielding. EUT_2 is a power converter (40 V to 16 V) module built into a test box used to investigate different EMI line filters. EUT_2 was part of the EMC studies for actual missions. The FMC-461 EMI input filter from Interpoint was connected. In both cases, the power converters operated without load.

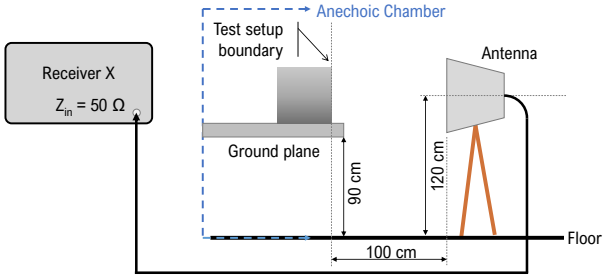

Fig. 3. Block diagram of the test setup: Experiment 2, RE testing.

C. The measuring receivers

The instruments used are a low-cost USB digitiser Picoscope PS5444D, a high-performance benchtop oscilloscope

TABLE I
DEFINITION OF MEASURING RECEIVERS USED IN THE EXPERIMENTS.

	Measuring instrument
Receiver 1, R_1	Picoscope 5444D + Software
Receiver 2, R_2	Rohde & Schwarz RTO6 + Software
Receiver 3, R_3	Rohde & Schwarz ESW44 (FFT scan mode)
Receiver 4, R_4	Rohde & Schwarz ESW44 (Swept mode)

R&S RTO6 and the R&S ESW44 full-compliant EMI test receiver as summarized in Table I.

Receivers 1 and 2 are based on direct-sampling instruments. They represent a subset of FFT-based receivers called Full Time-Domain EMI measurement systems. They are software-based implementations of an EMI receiver that can be adapted to the capabilities of general-purpose digitizing hardware, such as oscilloscopes. In this regard, after the interference/signal is sampled in baseband, the algorithms process the amplitude-discrete time-discrete waveforms for calculating the spectrum according to all the standard detectors [7]. For the sake of this article, only peak detection is used to measure the emission's spectrum as indicated in the ECSS standard. A block diagram of a multi-channel full time-domain EMI measurement system used during the experiments is shown in Fig. 4. Moreover, Table II summarises the key hardware specifications of the oscilloscopes employed.

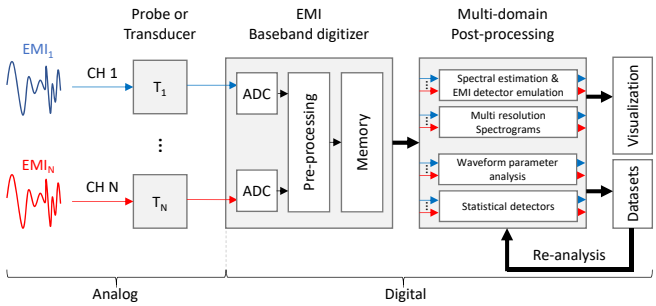

Fig. 4. Block diagram of the multi-channel full time-domain EMI measurement system used during the experiments [19].

Receivers 3 and 4 are the same instrument, the R&S ESW44 EMI test receiver, but used in FFT-mode and swept-mode. This high-end instrument is in line with CISPR 16-1-1, ANSI C63.2, MIL-STD-461 G and FCC standards. In FFT scan mode, its real-time bandwidth is 80 MHz. The software R&S EMC32 was used for running and automating the tests.

Finally, for all receiver's under consideration, the standard 6 dB resolution bandwidth and dwell times have been respected.

III. RESULTS

A. Verification of CE

Fig. 5 displays the spectrum of a multitone reference signal when measured with R_1, R_2 and R_3. The signal level injected was modulated in amplitude, so each tone is 6 dB below the limit line. For the final results, the RF current probe model

TABLE II
MAIN OSCILLOSCOPE SPECIFICATIONS USED AS PART OF THE MULTICHANNEL TIME-DOMAIN EMI MEASUREMENT SYSTEMS.

Spec.	PS5444D	R&S RTO64+B92
BW (-3 dB)	200 MHz	3 GHz
Resolution (Hardware + High-res)	Up to 16 bit + 4 bit; ENOB =(6.9;9.8)	Up to 16 bit; ENOB=(7.1;9.4)
Sampling frequency	Max. 1 GS/s @ 8 bit and 62.5 MS/s @ 16 bit. Single channel.	Max 10 GS/s per channel. Independent ADCs.
Input ranges	1 MΩ: ±10 mV to ±20 V full scale (External 50 Ω matching was required).	1 MΩ: 1 mV/div to 10 V/div and 50 Ω: 1 mV/div to 1 V/div.
Memory depth	512 MS @ 8 bit and 256 MS up to 16 bit.	200 MS/channel, 800 MS in total.
Num. Ch.	4	4
Spurious free dynamic range	Up to 12 bit: 60 dB; Up to 16 bit: 70 dB. At 100 kHz, full-scale input.	109 dB @ 1 GHz and 70 mV/div.
Noise	8 bit: 120 μV RMS; 12 bit: 110 μV RMS; 14-bit: 100 μV RMS; 15 bit: 85 μV RMS; 16 bit: 70 μV RMS; (on ±10 mV range).	0.13 mV RMS on the ±1 mV/div range.
Input impedance	1 MΩ ±1% ‖ 14 pF ±1 pF, 50 Ω ±3% (external adapter).	1 MΩ ±1% ‖ 15 pF, 50 Ω ±1.5%.

6741-1 was used from 50 kHz to 30 MHz and the probe 9145-1 was used for the 30 MHz to 100 MHz range. Each of those current probes performed better at different frequency ranges, and their calibration factors were more accurately known in the selected bands.

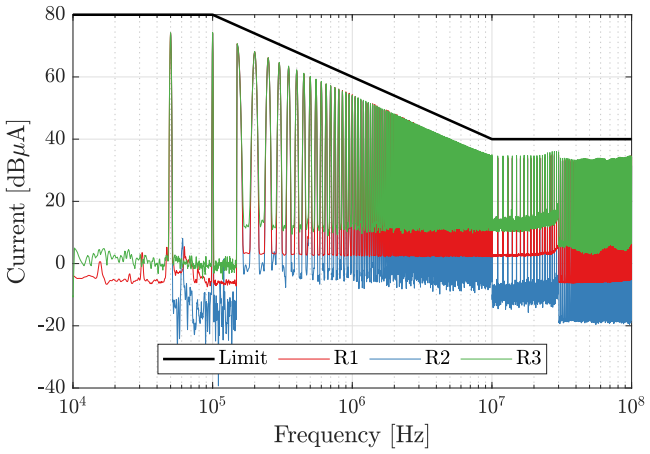

Fig. 5. Spectrum of the multitone reference signal.

The changes in resolution bandwidth at 150 kHz and 30 MHz can be observed in the spectrum where the noise level varies. Moreover, the effect of the different current probe sensitivities is noticeable in the noise floor variation below and above 30 MHz. From Fig. 5, a good agreement between the measurements of the different receivers can be inferred. This is confirmed if we zoom around specific frequencies as shown in Fig. 6 since the measured results are within ± 0.5 dB.

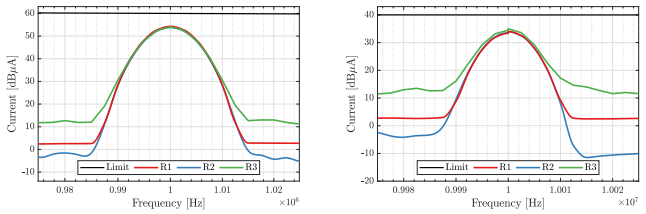

(a) Amplitude spectrum at 1 MHz. (b) Amplitude spectrum at 10 MHz.

Fig. 6. Comparison of the measured signal level at the exact frequencies required by the standard CE verification method.

However, a more detailed comparison is required to conclude. For this reason, the deviation of the measured signal level with respect to the expected one, ε, was calculated for all the peaks at the injected frequencies, that is,

$$\varepsilon(f = f_{\text{peaks}})[\text{dB}] = M_{\text{level}}[\text{dB}\mu\text{A}] - E_{\text{level}}[\text{dB}\mu\text{A}], \qquad (1)$$

where E_{level} and M_{level} are the expected and measured signal levels, respectively. This means that if $\varepsilon > 0$, the measured level is higher than the expected one. Conversely, if $\varepsilon < 0$, the registered signal level is lower than the reference voltage at that particular frequency. Fig. 7 plots ε for R_1, R_2, and R_3.

Below 30 MHz, all receivers delivered very accurate results, with mean deviations of -0.11 dB, 0.34 dB and 0.21 dB for R_1, R_2 and R_3, respectively. When comparing the results from R_1 with the other two receivers, it is evident that ε is more variable. This effect might be related to a worse input impedance matching of R_1, since the oscilloscope required an external adaptor for 50 Ω. Above 20 MHz, there is a clear systematic effect that increases ε, and, in this case, the cause is likely related to current probe calibration factors. This outcome should be further investigated in the future. For frequencies above 30 MHz, R_3 is superior to R_1 and R_2. Nonetheless, it is possible that the larger deviations encountered in R_2 for $f > 50$ MHz are due to a misuse of the HD feature of the RTO6 that could have introduced unintended and limiting effects. The good results obtained with the low-cost PS5444D, even in the higher frequency range, must be highlighted. The mean deviation difference of R_1 with respect to the results from the R_3 (ESW44) is about 1 dB for $f > 30$ MHz.

In general, the experiment showed the accuracy and precision of the different instruments are suitable for the CE test application, provided some systematic errors are corrected. This is evident in Fig. 8 since all three histograms have most of the area in the $|\varepsilon| \leq 1$ dB region. For a contextualized interpretation of the results, we must remember the data

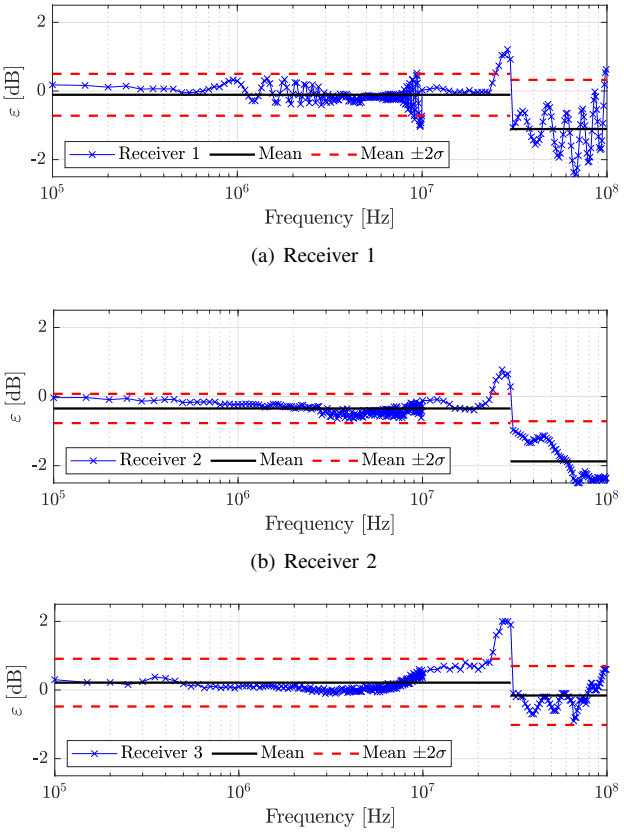

(a) Receiver 1

(b) Receiver 2

(c) Receiver 3

Fig. 7. Deviation of the measured voltage levels at the peak frequencies with respect to the expected value of the injected multitone signal. (a) Receiver 1; (b) Receiver 2; (c) Receiver 3. Note: Above 30 MHz, ε increases significantly. This is likely related to larger uncertainty in the current probe factors.

reported was not obtained under receiver calibration conditions but using the actual CE test verification setup. Therefore, the errors due to the combination of setup elements should be considered contributors to the measurement uncertainty.

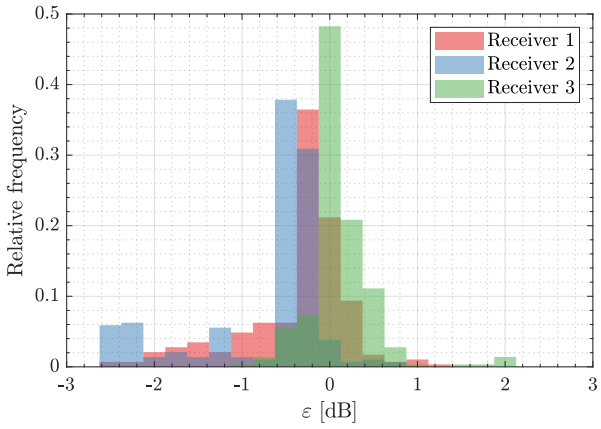

Fig. 8. Distribution of the deviation of the measured voltage levels at the peak frequencies with respect to the expected value of the injected multitone signal per receiver model.

B. CE Testing

Fig. 9 presents the results from the differential mode current measured using the test setup for CE emissions. On the left-hand side, there are the results for EUT_1, while on the right-hand side, the corresponding outcome for EUT_2. The results are presented in the 150 kHz - 100 MHz range. Below 150 kHz, no relevant emissions were detected. Again, the results of all receivers are in good agreement regarding the spectrum amplitude level, which is predominantly populated by the harmonics of the switching frequency.

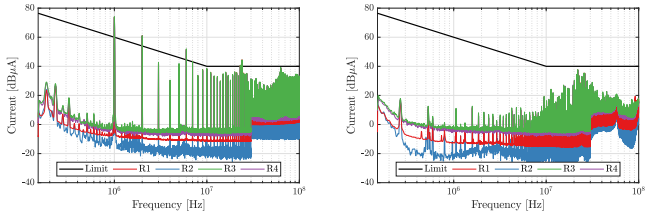

(a) EUT_1. (b) EUT_2.

Fig. 9. Comparison of the differential-mode CE emissions of DC/DC power converter modules measured with the test receivers considered.

To visualize the correlation between the results more clearly, the peaks have been extracted and plotted versus frequency in a linear scale (Fig. 10). Then, the correlation coefficient between pairs of CE measurements, ρ, was calculated, delivering the results in Table III.

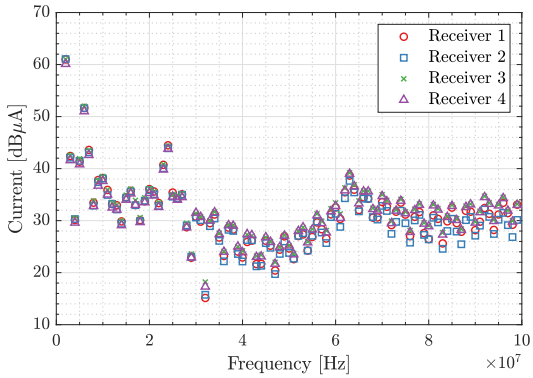

Fig. 10. Comparison of the differential-mode CE emissions of EUT_1 at the harmonic frequencies of 1 MHz.

TABLE III
CORRELATION BETWEEN PAIRS OF CE MEASUREMENTS WITH DIFFERENT TEST RECEIVERS.

ρ	R_1	R_2	R_3	R_4
R_1	1	0.9938	0.9950	0.9923
R_2	0.9938	1	0.9911	0.9868
R_3	0.9950	0.9911	1	0.9987
R_4	0.9923	0.9868	0.9987	1

Due to space limitations, this analysis is presented only for EUT_1 results. However, both cases exhibited a notably high correlation between all measuring receivers.

C. RE Testing

Fig. 11 corresponds to the E-field emissions from the EUT_1 measured with the antenna in the horizontal orientation. Data from the vertical polarization measurements are also available, but such results were omitted due to paper length restrictions.

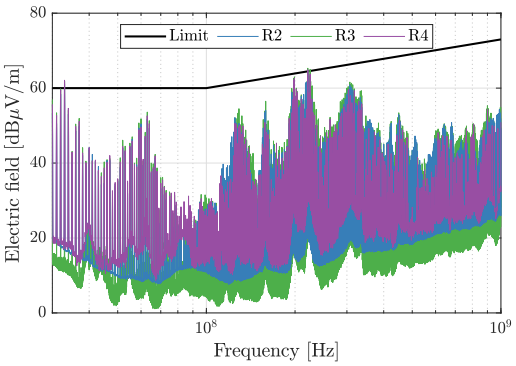

Fig. 11. E-field emissions measured with the antenna in the horizontal polarization. EUT_1.

The radiated emission test results are always the most complicated to compare with each other. One reason is the radiated emissions are more sensitive to minor changes in the setup. This is even more critical when measurements are conducted at a short distance between the EUT and the antenna. Moreover, the EUT emissions were slightly changing over time as the switching transistors of the power buck converter warmed up. In this case, the FFT-based receivers (R_2 and R_3) got higher emission levels overall. The electromagnetic disturbance produced by the EUT is intrinsically broadband, and for this reason, having broadband measurement capabilities is convenient to get complete information with every acquisition. The analysis of the measured peak emissions is shown in Fig. 12.

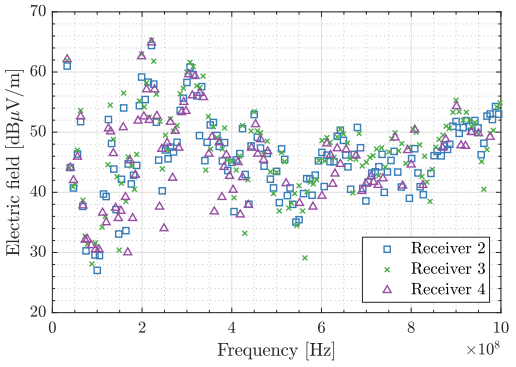

Fig. 12. Comparison of the E-field peak emissions of EUT_1.

In this case, developing the correlation analysis would not yield conclusive results. One reason is the peaks often did not coincide one-to-one in the frequency axis because of the different steps. However, it is clear all instruments delivered consistent information, and most importantly, they matched at those frequencies where emissions are ± 6 dB from the limit.

IV. Conclusions

This empirical study allowed us to compare the measurements obtained with different EMI receivers. It is relevant because the experimental conditions are close to actual testing scenarios for space applications; thus, factors not present during typical calibrations emerge. Therefore, the results are more representative of the expected similarities and divergences found in practice. Generally, the instruments based on direct sampling delivered good and coherent results compared to the high-end receiver with the FFT scan and the swept modes. Still, when measuring CE with oscilloscopes, the band-limiting effect of high-definition modes must be considered to prevent systematic errors. In all cases, the selected oscilloscopes had suitable dynamic range and accuracy to deliver equivalent conclusions. There are still some open questions requiring further investigations, e.g. deviations above 20 MHz. Nevertheless, given the promising results obtained so far, it is recommended to take advantage of the wide availability of oscilloscopes for doing early EMI checks, supporting the electronic design teams at pre-compliance stages, and streamlining compliance evaluation to meet the standard requirements.

Acknowledgment

The project (21NRM06 EMC-STD) has received funding from the European Partnership on Metrology, co-financed by the European Union's Horizon Europe Research and Innovation Programme and by the Participating States.

EMC Barcelona's project under grant number SNEO-20211223 has received funding from CDTI, which is supported by "Ministerio de Ciencia e Innovación" and financed by the European Union – NextGenerationEU – through the guidelines included in the "Plan de Recuperación, Transformación y Resiliencia".

Dr. Azpúrua has received funding from the StandICT.eu 2023 project, financed by the European Union's Horizon Europe - Research and Innovation Programme - under grant agreement no. 951972.

Dr. Pous work was supported in part by European Union's Horizon 2020 research and innovation programme under Marie Skłodowska-Curie grant agreement No. 801342 (TecniospringINDUSTRY) and the Government of Catalonia's Agency for Business Competitiveness (ACCIÓ) and in part by the Spanish "Ministerio de Ciencia e Innovación" under project PID2019-106120RBC31/AEI/10.13039/501100011033.

References

[1] "CISPR 16-1-1:2019 Ed 5.0. Specification for radio disturbance and immunity measuring apparatus and methods - Part 1-1: Radio disturbance and immunity measuring apparatus - Measuring apparatus," IEC, Geneva, CH, Standard, Jun. 2019.

[2] "ECSS-E-ST-20-07C Rev. 2. Space engineering – Electromagnetic Compatibility," ESA-ESTEC, European Cooperation for Space Standardization., Noordwijk, NL, Standard, Jan. 2022.

[3] M. A. Azpúrua, M. Pous, and F. Silva, "A Measurement System for Radiated Transient Electromagnetic Interference based on General Purpose Instruments," in *2015 IEEE International Symposium on Electromagnetic Compatibility (EMC)*, 2015. doi: 10.1109/ISEMC.2015.7256338 pp. 1189–1194.

[4] M. Pous, M. A. Azpúrua, and F. Silva, "Measurement and Evaluation Techniques to Estimate the Degradation Produced by the Radiated Transients Interference to the GSM System," *IEEE Transactions on Electromagnetic Compatibility*, vol. 57, no. 6, pp. 1382–1390, 2015. doi: 10.1109/TEMC.2015.2472983

[5] S. Braun, T. Donauer, and P. Russer, "A Real-Time Time-Domain EMI Measurement System for Full-Compliance Measurements According to CISPR 16-1-1," *IEEE Transactions on Electromagnetic Compatibility*, vol. 50, no. 2, pp. 259–267, 2008. doi: 10.1109/TEMC.2008.918980

[6] M. Keller, "A New Concept for a Wideband FFT-Based EMI Receiver," in *2022 ESA Workshop on Aerospace EMC*, 2022. doi: 10.23919/AerospaceEMC54301.2022.9828846 pp. 1–5.

[7] M. A. Azpúrua, M. Pous, S. Çakir, M. Çetinta, and F. Silva, "Improving Time-domain EMI measurements through Digital Signal Processing," *IEEE EMC Magazine*, vol. 4, no. 2, pp. 82–91, 2015. doi: 10.1109/MEMC.2015.7204056

[8] M. A. Azpúrua, M. Pous, and F. Silva, "On-board compact system for Full Time-domain Electromagnetic Interference Measurements," in *2016 ESA Workshop on Aerospace EMC*, 2016. doi: 10.1109/AeroEMC.2016.7504579 pp. 1–4.

[9] C. Spindelberger and H. Arthaber, "Out-of-the-Box Performance of popular SDRs for EMC pre-compliance Measurements," in *2022 International Symposium on Electromagnetic Compatibility – EMC Europe*, 2022. doi: 10.1109/EMCEurope51680.2022.9901003 pp. 677–682.

[10] C. Spindelberger and H. Arthaber, "Improving the Performance of Direct-Conversion SDRs for Radiated Pre-Compliance Measurements," *IEEE Letters on Electromagnetic Compatibility Practice and Applications*, pp. 1–1, 2022. doi: 10.1109/LEMCPA.2022.3227409

[11] R. Gomez, "Theoretical Comparison of Direct-Sampling Versus Heterodyne RF Receivers," *IEEE Transactions on Circuits and Systems I: Regular Papers*, vol. 63, no. 8, pp. 1276–1282, 2016. doi: 10.1109/TCSI.2016.2564680

[12] M. A. Azpúrua, M. Pous, J. A. Oliva, B. Pinter, M. Hudlička, and F. Silva, "Waveform Approach for Assessing Conformity of CISPR 16-1-1 Measuring Receivers," *IEEE Transactions on Instrumentation and Measurement*, vol. 67, no. 5, pp. 1187–1198, 2018. doi: 10.1109/TIM.2018.2794941

[13] M. A. Azpúrua, M. Pous, and F. Silva, "Specifying the Waveforms for the Calibration of CISPR 16-1-1 Measuring Receivers," *IEEE Transactions on Electromagnetic Compatibility*, vol. 62, no. 3, pp. 654–662, 2020. doi: 10.1109/TEMC.2019.2923813

[14] J. Hernandez and M. Owen, "CISPR 32 — Conducted Emissions Test Benchmarking Using Automated FFT & Stepped-Based Systems," in *2019 International Symposium on Electromagnetic Compatibility - EMC EUROPE*, 2019. doi: 10.1109/EMCEurope.2019.8871765 pp. 544–549.

[15] M. Pous, M. Azpúrua, and F. Silva, "Benefits of full time-domain EMI measurements for large fixed installation," in *2016 International Symposium on Electromagnetic Compatibility - EMC EUROPE*, 2016. doi: 10.1109/EMCEurope.2016.7739221 pp. 514–519.

[16] M. Pous, M. A. Azpúrua, J. A. Oliva, M. Aragón, I. González, and F. Silva, "Full Time Domain EMI Measurement System Applied to Railway Emissions According to IEC 62236-3-1/EN 50121-3-1 Standards," in *2018 International Symposium on Electromagnetic Compatibility (EMC EUROPE)*, 2018. doi: 10.1109/EMCEurope.2018.8485173 pp. 260–265.

[17] M. Bosi, A.-M. Sánchez, F. Pajares, I. García, J. Accensi, and J. Regué, "Common- and Differential-Mode Conducted Emissions Measurements using Conventional Receivers versus FFT-Based Receivers," *IEEE Electromagnetic Compatibility Magazine*, vol. 11, no. 3, pp. 55–63, 2022. doi: 10.1109/MEMC.2022.9982541

[18] "MIL-STD-461G. Requirements for the control of electromagnetic interference characteristics of subsystems and equipment," Department of Defense, USA, Standard, Dec. 2015.

[19] M. Pous, D. Zhao, M. A. Azpúrua, T. Bozhanov, F. Silva, and J. Wolf, "Time-Domain Electromagnetic Characterization of Reaction Wheel for Space Applications," *IEEE Transactions on Electromagnetic Compatibility*, pp. 1–11, 2023. doi: 10.1109/TEMC.2022.3227368

[20] J. Medler and M. J. Lorenzo, "EMI Testing on Space Systems - Use of FFT-Based Measuring Receivers for More Speed, More Insight and Better Reliability," in *2022 ESA Workshop on Aerospace EMC*, 2022. doi: 10.23919/AerospaceEMC54301.2022.9828860 pp. 01–05.